ACS APPLIED MATERIALS & INTERFACES

Research Article

www.acsami.org

DNA-Length-Dependent Quenching of Fluorescently Labeled Iron Oxide Nanoparticles with Gold, Graphene Oxide and MoS_2 Nanostructures

Mustafa Balcioglu,[†] Muhit Rana,[†] Neil Robertson,[†] and Mehmet V. Yigit*[,†,‡]

[†]Department of Chemistry and RNA Institute, University at Albany, SUNY, 1400 Washington Avenue, Albany, New York 12222, United States

[‡]College of Nanoscale Science & Engineering, University at Albany, SUNY, 257 Fuller Road, Albany, New York 12203, United States

Supporting Information

ABSTRACT: We controlled the fluorescence emission of a fluorescently labeled iron oxide nanoparticle using three different nanomaterials with ultraefficient quenching capabilities. The control over the fluorescence emission was investigated via spacing introduced by the surface-functionalized single-stranded DNA molecules. DNA molecules were conjugated on different templates, either on the surface of the fluorescently labeled iron oxide nanoparticles or gold and nanographene oxide. The efficiency of the quenching was determined and compared with various fluorescently labeled iron oxide nanoparticle and nanoquencher combinations using DNA molecules with three different lengths. We have found that the template for DNA conjugation plays significant role on quenching the fluorescence emission of the fluorescently labeled iron oxide nanoparticles. We have observed that the size of the DNA controls the quenching efficiency when conjugated only on the fluorescently labeled iron oxide nanoparticles by setting a spacer between the surfaces and resulting change in the hydrodynamic size. The quenching efficiency with 12mer, 23mer and 36mer oligonucleotides decreased to 56%, 54% and 53% with gold nanoparticles, 58%, 38% and 32% with nanographene oxide, 46%, 38% and 35% with MoS_2, respectively. On the other hand, the presence, not the size, of the DNA molecules on the other surfaces quenched the fluorescence significantly with different degrees. To understand the effect of the mobility of the DNA molecules on the nanoparticle surface, DNA molecules were attached to the surface with two different approaches. Covalently immobilized oligonucleotides decreased the quenching efficiency of nanographene oxide and gold nanoparticles to ~22% and ~21%, respectively, whereas noncovalently adsorbed oligonucleotides decreased it to ~25% and ~55%, respectively. As a result, we have found that each nanoquencher has a powerful quenching capability against a fluorescent nanoparticle, which can be tuned with surface functionalized DNA molecules.

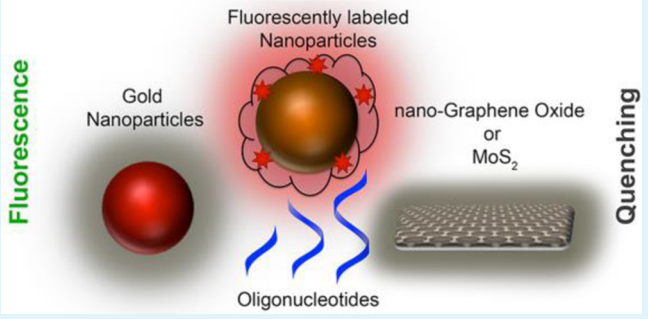

KEYWORDS: *graphene oxide, MoS_2, iron oxide, gold, nanoparticle, DNA*

1. INTRODUCTION

Nanotechnology has developed remarkably over the last two decades. One of the most multidisciplinary active areas of research is the construction of functional biomaterial and nanoparticle conjugates.[1−3] Development of novel nanomaterials has provided a simple yet notable translation of biological knowledge into applied science.[4,5] For instance, attachment of oligonucleotides with different sequences and lengths on a nanoparticle surface has been a routine approach for most of the practical applications. A variety of nanoparticles coated with oligonucleotides have been used as biomedical diagnostic tools,[6−9] vectors for drug delivery and gene therapy,[10−12] or templates for biosensors.[13−16] Despite the countless potential of nanomaterials in bioscience, multiple factors have to be controlled carefully because some interfacial interactions in biological environments can influence the function of the nanomaterials dramatically.[17−19] One important parameter is the gap introduced by biomaterials between the interfaces of nanostructures.[20−23] For example, in DNA functionalized nanoparticles, the oligonucleotides participate in the spacing between the surfaces of the nanoparticle and the targeted material. However, the magnitude of spacing may not always be proportional to the size of the DNAs on the surface. Here, we investigated the effect of distance, introduced by short single-stranded (ss)DNA molecules, on controlling the fluorescence of fluorescently labeled iron oxide nanoparticles with graphene oxide, MoS_2, and gold nanoparticles.

Nanographene oxide (nGO), a two-dimensional honeycomb shaped Carbon material, has been studied extensively in recent years due to its attractive mechanical, electrical, thermal and

Received: February 24, 2014
Accepted: July 11, 2014
Published: July 11, 2014

optical properties.[24−27] nGO has remarkable potential in biomedical applications[28] due to its exceptional ssDNA adsorption[29] and ultraefficient fluorescence quenching capabilities.[30−32] These properties have attracted significant attention to nGO for biosensor development,[33−41] biomarker detection[42,43] and antisense gene delivery.[44−46] Currently, DNA functionalized graphene-based systems are under heavy investigation for numerous purposes,[4] including engineering functional hybrid nanostructures.[31] Therefore, the interaction of the interfaces of DNA functionalized nGOs needs to be studied carefully for construction of graphene-based biosystems. MoS_2, which is a two-dimensional graphene-like material, has recently received great attention due to its exciting physical properties comparable to nGO.[50] It has been used for nanoelectronics, optoelectronics, transistor designs, energy storing devices and biosensing systems.[47,48] Similar to nGO, MoS_2 quenches the fluorescence of fluorophore labeled materials, which makes them attractive two-dimensional nanosized templates for photonic or biomedical applications.[49]

Gold nanoparticles (AuNP) have several common properties with nGO and MoS_2 regardless of the entirely different three-dimensional structure and elemental composition. Gold nanoparticles have been studied considerably due to their unique physical properties.[50−52] Several analytical and biomedical studies have demonstrated that (1) both AuNP and nGO are ultraefficient fluorescence quenchers[53−56] and (2) ssDNA molecules can be immobilized or adsorbed on both surfaces very efficiently via specific chemical interactions or aromatic stacking.[57−60] Because the attachment of DNA molecules constructs a biological shield on the surface of these two nanoparticles, nanoquenchers, we investigated whether this barrier can be used to control the fluorescence emission of a fluorescent nanoparticle.

Dextran coated fluorescently labeled iron oxide nanoparticles are a class of imaging agents that are suitable for biomedical applications.[61−63] They have been used for many different applications including whole body in vivo optical and MRI imaging.[8,64] The strong NIR fluorescence signals of these nanoparticles ($MN_{cy5.5}$ − cy5.5 dye labeled form) provide noninvasive optical tissue imaging in live animals. The attachment of siRNA or antisense miRNA molecules provides additional therapeutic functionality, which makes these nanoparticles attractive particularly for theranostics.[65] Due to its multiple functionalities along with the biocompatible and biodegradable nature, $MN_{cy5.5}$ has been one of the major tools for theranostics in biomedicine.[66,67] Here, we controlled the fluorescence emission of $MN_{cy5.5}$ using nGO, MoS_2 and AuNPs, promising theranostic nanomaterials, with surface-functionalized ssDNA molecules. The covalently or noncovalently attached ssDNA molecules on the nanoparticle surface serve as biological shields between the interfaces, which could increase the hydrodynamic sizes of the nanoparticles.

Although significant effort has been devoted to study the biophysical properties and the applications of individual oligonucleotide-functionalized nanoparticles, their interaction with other nanoparticle types with systematic spacing has not been investigated in depth.[20−23] We observed that the surface bound short ssDNA molecules interfere with the interaction between nanoparticle interfaces however the length of the DNA does not always determine the degree of interaction. We believe that the coverage and orientation of DNA molecules on the surface, and the three-dimensional structures of the nanomaterials, could be important factors in their biophysicochemical interfacial interactions.

2. EXPERIMENTAL SECTION

2.1. Materials. All DNA sequences were purchased from Integrated DNA Technologies (IDT), Coralville, IA, USA, with the following sequence information and modifications, Thiol modified sequences: (1) 12mer, 5′- /5ThioMC6-D/ CCC AGG TTC TCT -3′; (2) 23mer, 5′- /5ThioMC6-D/ CAC AAA TTC GGT TCT ACA GGG TA-3′; (3) 36mer, 5′- /5ThioMC6-D/ TAC GAG TTG AGA CCG TTA AGA CGA GGC AAT CAT GCA-3′. Amine modified sequences: (4) 12mer, 5′- /5AmMC6/ CCC AGG TTC TCT -3′; (5) 23mer, 5′- /5AmMC6/ CAC AAA TTC GGT TCT ACA GGG TA-3′; (6) 36mer, 5′- /5AmMC6/ TAC GAG TTG AGA CCG TTA AGA CGA GGC AAT CAT GCA-3′. (7) Mercury Aptamer, 5′- /TTC TTT CTT CCC CTT GTT TGT T-3′.

Carboxyl graphene water dispersion was purchased from ACS Material, Medford, MA, USA. Dextan-T10 was purchased from Pharmacosmos, Holbaek, Denmark. cy5.5 monoreactive NHS ester was purchased from GE Healthcare, Piscataway, NJ, USA. MoS_2 powder (<2 μm) was purchased from Sigma-Aldrich. All other reagents were purchased form from Sigma-Aldrich, St. Louis, MO, USA, and used without further purification. Double distilled water was used in preparation of all solutions.

2.2. Synthesis of cy5.5 Labeled Iron Oxide Nanoparticles and Functionalization with Oligonucleotides. Synthesis of iron oxide nanoparticle (MN) was adapted from our earlier publication.[31] The cy5.5 monoreactive NHS ester (1 mg) was dissolved in 200 μL of dimethyl sulfoxide (DMSO) and incubated with 1 mL of the nanoparticles (MN, 10.0 mg/mL Fe) in 20 mM sodium citrate buffer (pH 8.0) overnight. The labeled nanoparticles ($MN_{cy5.5}$) were purified using Sephadex PD-10 column (GE Healthcare) against 10 mM phosphate buffered saline (PBS, pH 7.4). The number of cy5.5 dye molecules per nanoparticle was determined as 10−12 by UV spectroscopy as described previously.[68] The hydrodynamic size of nanoparticle was determined as 33.1 (±4.1 nm) using dynamic light scattering (DLS) measurements with DynaPro Titan (Wyatt Technology Corporation, Goleta, CA, USA).

The covalent conjugation of DNA to $MN_{cy5.5}$ was performed through a heterobifunctional linker SPDP (N-succinimidyl 3-(2-pyridyldithio)propionate)[68,69] purchased from Pierce Biotechnology, Rockford, IL, USA. Briefly, 10 mg of succinimidyl 3-(2-pyridyldithio)-propionate (SPDP) was dissolved in 500 μL of anhydrous DMSO and incubated with $MN_{cy5.5}$. The thiolated 5′ terminus of the oligonucleotides was activated with 3% tris(2-carboxyethyl)phosphine) (TCEP) treatment in nuclease-free 10 mM PBS (pH 7.4). The DNA molecules were purified using microspin G-25 columns (GE Healthcare). After TCEP-activation and purification, the oligonucleotides were resuspended in 10 mM PBS (pH 7.4) and incubated with the SPDP conjugated $MN_{cy5.5}$ overnight. The resulting probe was purified using a disposable MACS separation magnetic columns; Miltenyi Biotec Inc., Auburn, CA, USA. The DNA per $MN_{cy5.5}$ was prepared in a 10:1 molar ratio as described previously.[68]

2.3. Synthesis of Gold Nanoparticles and Functionalization with Oligonucleotides. The negatively charged citrate-stabilized gold nanoparticles were synthesized and functionalized with oligonucleotides according to previous reports.[70] Briefly, 2 mL of 50 mM $HAuCl_4$ was added into 98 mL of boiling DI water in an Erlenmeyer flask on a hot plate. 10 mL of 38.8 mM sodium citrate solution was rapidly added into the stirring mixture. The reaction is stopped until the solution turned a wine-red color. The solution was cooled to room temperature and stored at 4 °C. The hydrodynamic size of nanoparticle was determined as 13 nm (±1.4 nm) using dynamic light scattering (DLS) measurements with DynaPro Titan (Wyatt Technology Corporation, Goleta, CA, USA).

Immobilization of Oligonucleotides on AuNP. 10 μL of 1 mM TCEP-treated thiol-modified DNA molecules was incubated with 3 mL of AuNP overnight at room temperature (RT).[70] Next, 100 mM NaCl was added into the DNA and AuNP mixture with gentle stirring.

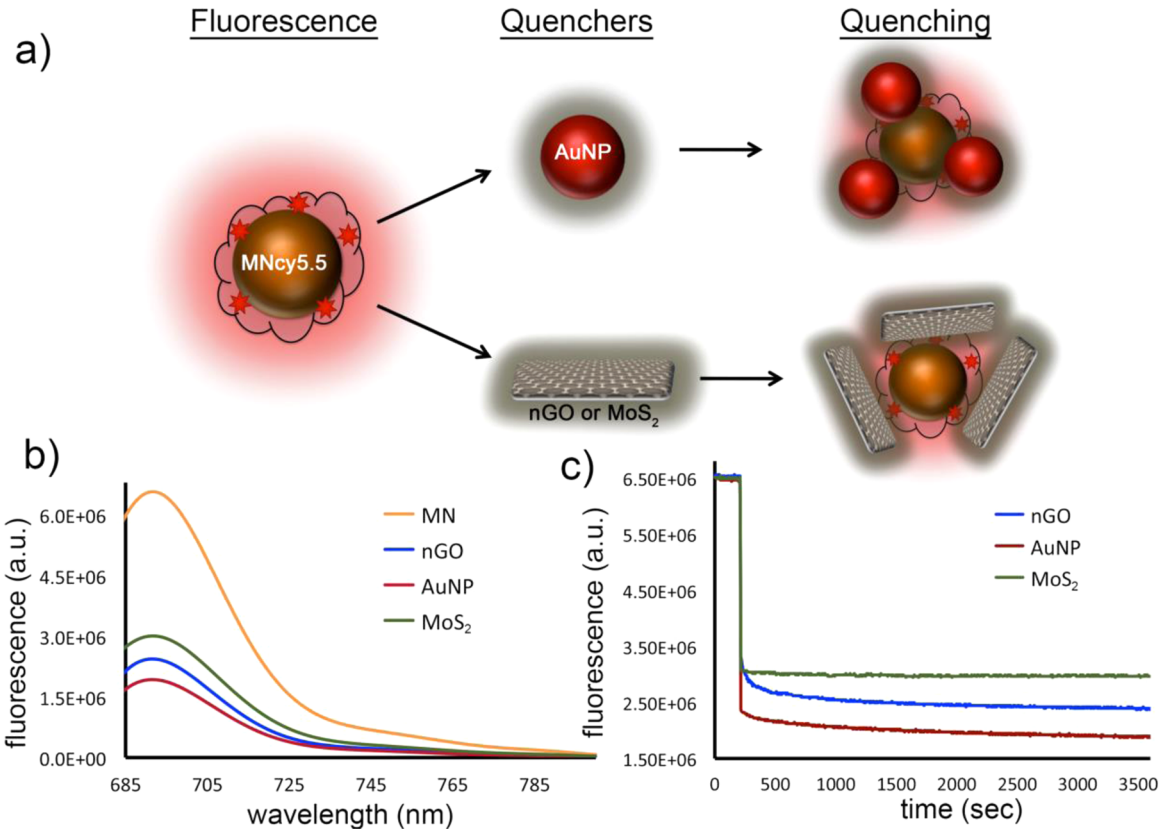

Figure 1. AuNP, nGO or MoS_2 quenches the fluorescence emission of cy5.5 labeled iron oxide nanoparticles, $MN_{cy5.5}$. (a) A schematic representation of the interaction between the $MN_{cy5.5}$ and nanoquenchers demonstrates the quenching of the cy5.5 fluorophore on $MN_{cy5.5}$. (b) Fluorescence emission spectra of 20 nM $MN_{cy5.5}$ (orange line) with 4 nM AuNP (red line), 1.8 μg/mL nGO (blue line) or 20 μg/mL MoS_2 (green line). (c) Titration of $MN_{cy5.5}$ with AuNP, nGO or MoS_2 at 200th second of the time-dependent fluorescence measurements at 695 nm. The fluorescence signals were quenched immediately upon titration with nanoquenchers and stabilized with no significant change overtime.

The samples were stored in the dark for 24 h. The samples were then centrifuged at 15000 rpm for 15 min at RT. The supernatant was removed and discarded. The AuNP−DNA conjugate at the bottom of the microcentrifuge tube was dispersed in 100 mM PBS (pH 7.4) and 150 mM NaCl. The samples were washed and centrifuged two times to ensure complete removal of free DNA. Finally, the AuNP−DNA conjugate was resuspended in 100 mM PBS (pH 7.4) and 150 mM NaCl.

Noncovalant Adsorption of Oligonucleotides on AuNP. 2.5 μL of 1 mM unmodified DNA stock solution was dissolved in 50 μL of 100 mM MES buffer (pH 5.6). The DNA solution was then added to 450 μL of citrate-stabilized AuNPs. After 20 min of incubation at RT, MES buffer pH 5.6 (final conc. 10 mM MES, 100 mM NaCl) was added to stabilize the DNA adsorption on AuNP. The sample was incubated for another 10 min. Finally, the DNA−AuNP mixture was centrifuged at 15000 rpm, and the supernatant was discarded. The pellet was washed with 10 mM PBS pH 7.4 to remove any excess free DNA. The centrifugation and washing procedure was repeated two times to ensure complete removal of free DNA. Finally AuNP-DNA conjugate was resuspended in 100 mM PBS (pH 7.4) and 150 mM NaCl.

Mercury detection was performed with 2.5 μL of 1 mM mercury aptamer incubated with or without 1 μM mercury(II) perchlorate for 10 min. The aptamer solutions were incubated with 450 μL of citrate-stabilized AuNPs for 20 min. After the washing steps, the $MN_{cy5.5}$ suspension was titrated with AuNPs and the fluorescence was measured as described below.

2.4. Preparation of Nanographene Oxide (nGO) and MoS_2 via Sonication and Functionalization with Oligonucleotides. To prepare nanometer sized GO (0.5 mg/mL) and MoS_2 (0.5 mg/mL), the starting materials were dispersed in DI water and sonicated with the ultrasonic processor for 7 h (120 W 20 kHz with pulse on for 2 s and pulse off for 4 s) in an ice bath to prevent overheating generated from sonication. The average particle size of the obtained nGO and MoS_2 was determined as 100 ± 15 nm using dynamic light scattering (DLS) DynaPro Titan (Wyatt Technology Corporation, Goleta, CA, USA). The transmission electron microscopy (TEM) micrographs were taken using a JEOL JEM-2010 transmission electron microscope. The characterization of each nanomaterial is provided in Figure S8 (Supporting Information).

Immobilization of Oligonucleotides on nGO. The coupling reaction was carried out in a glass vial with 200 μL of 500 μg/mL nGO, 2 μL of 1 mM amine-modified DNA, 2 mg of EDC (*N*-(3-(dimethylamino)propyl)-*N*′-ethylcarbodiimide hydrochloride) and 25 mM MES (pH 5.6) and 25 mM NaCl.[23] The mixture was rotated at RT for 3 h using a Glas-Col mini rotator. The solutions were centrifuged at 15000 rpm for 20 min to remove nonattached DNAs. The GO−DNA conjugates were then washed with 500 μL of DI water twice to further remove nonassociated DNAs. Finally, the conjugates were redispersed in 1 mL of 25 mM (4-(2-hydroxyethyl)-1-piperazineethanesulfonic acid) (HEPES), 100 mM NaCl (pH 7.6) and with a final nGO concentration of 100 μg/mL. The samples were stored at 4 °C before use. Sonication was performed occasionally to assist redispersing.

Noncovalent Adsorption of Oligonucleotides on nGO. 2 μM of DNA was incubated with nGO (100 μg/mL) in buffer (25 mM HEPES, 100 mM NaCl, pH 7.6) for 1 h at RT.[23] Nonadsorbed DNAs were removed by centrifugation and washing cycles as described above. Finally, the purified nGO−DNA complex was resuspended in buffer (25 mM HEPES, 100 mM NaCl, pH 7.6).

2.5. Fluorescence Measurements. The fluorescence measurements (excitation, 670 nm; emission, 695 nm) were performed using the Fluorolog-3 spectrofluorometer (Horiba Jobin-Yvon, Inc., Edison, NJ, USA). A typical experiment was performed with 20 nM $MN_{cy5.5}$ in

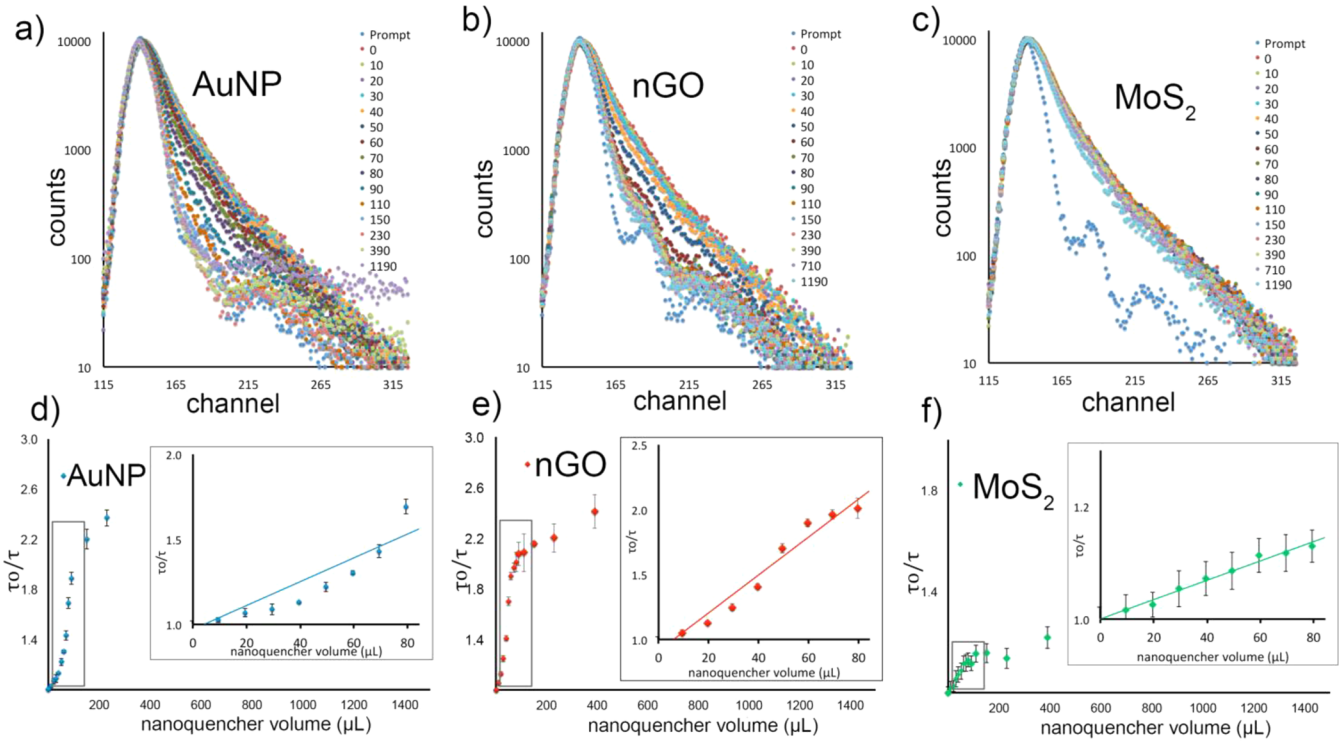

Figure 2. Fluorescence lifetime decay traces of $MN_{cy5.5}$ with different concentrations of (a) AuNP, (b) nGO and (c) MoS_2. Stern–Volmer plots of (d) AuNP,(e) nGO and(f) MoS_2 show a linear correlation in the insets. Time calibration =5.578 023 × 10^{-2} nanosecond/channel. Note: the concentration vs volume table is provided in Figure S1 (Supporting Information). Nanoquencher volume: 10 μL of stock MoS_2 (620 μg/mL), nGO (72 μg/mL) and AuNP (84 nM) solution is equivalent to 3.1 μg/mL, 0.4 μg/mL and 0.4 nM final concentrations, respectively.

10 mM PBS (pH 7.4) in a 2 mL quartz cuvette with gentle stirring. The fluorescence emission value at this concentration was determined to be approximately ~6.5 × 10^6. The kinetic studies on $MN_{cy5.5}$ were performed on for 30 min with one reading per 3 s resolution. At the 200 s time point, 1.8 μg/mL of nGO, 20 μg/mL of MoS_2 or 4 nM of AuNP was added into the $MN_{cy5.5}$ to monitor the quenching efficiency of these nanomaterials on the fluorescence of $MN_{cy5.5}$.

The quenching efficiency was calculated according to following equation.[23] $Q\ (\%) = [1 - F_o/F]$ where Q is the quenching efficiency, F_o is the fluorescence intensity in the absence of quencher and F is the fluorescence intensity in the presence of quencher.

Fluorescence lifetime measurements were performed on $MN_{cy5.5}$ with nGO, MoS_2 and AuNPs using time-correlated single-photon counting (TCSPC) spectroscopy on Fluorolog Horiba Jobin Yvon equipment with NanoLED ($\lambda = 635 \pm 10$ nm) excitation sources. The fluorescence lifetime values were analyzed by deconvoluting the instrument response function with biexponential decay using DAS6 decay analysis software. The quality of the fit has been judged by the fitting parameters such as $\chi 2$ (<1.2). Stern–Volmer Plots were determined by τ_0/τ vs concentration of nanoquenchers.

3. RESULTS AND DISCUSSION

Here, we investigated the interaction of AuNP, nGO or MoS_2 with fluorescently labeled iron oxide nanoparticles ($MN_{cy5.5}$) in a distance-dependent manner using fluorescence spectroscopy. The spacing between the species was controlled using short ssDNA molecules, which changed the hydrodynamic size of the nanoparticles or served as biological shields between interfaces. Comparisons were made between two nanomaterials; one serving as fluorescence quenchers, nanoquenchers: AuNPs, nGO or MoS_2, and the other, $MN_{cy5.5}$, serving as a fluorescence carrier.

First, we investigated the quenching of bare $MN_{cy5.5}$ with nGO, MoS_2 or AuNP, (Figure 1a). $MN_{cy5.5}$ presents a strong steady fluorescence at pH 7.4, (Figure 1b). After the titration with nGO, MoS_2 or AuNP solutions, significantly weaker fluorescence emission was observed due to fluorescence quenching, (Figure 1b). The emission spectra were collected on 20 nM $MN_{cy5.5}$ before and after the titration with 1.8 μg/mL nGO, 4 nM AuNP or 20 μg/mL MoS_2. These nanoquencher concentrations were determined to be ideal for obtaining the optimum quenching yield with a minimum nanoquencher concentration, Figure S1 (Supporting Information). Beyond these concentrations, slightly higher fluorescence quenching was observed; however, the nanoquencher concentrations in these emission ranges were dramatically higher, particularly for MoS_2. This effect could be due to the saturation of the $MN_{cy5.5}$ fluorescence emission environment with the nanoquenchers in the solution.

The kinetics studies were performed similarly by titration of $MN_{cy5.5}$ with AuNP, nGO or MoS_2 suspension and monitored for 1 h. It has been previously shown that the bare nGO, AuNP and $MN_{cy5.5}$ interact with each other through electrostatic interaction, which leads to an immediate quenching of the fluorescence.[31] As seen in Figure 1c, the fluorescence was quenched immediately and stabilized shortly after the nanoquencher titration without any major fluctuation. We observed that AuNP, nGO and MoS_2 have similar quenching performance on $MN_{cy5.5}$ fluorescence in this experimental condition. The fluorescence lifetime measurements were performed on $MN_{cy5.5}$ with different concentrations of AuNP, nGO or MoS_2 as seen in Figure 2. The results showed that the nanoquenchers result in a decrease in the fluorescence lifetime of $MN_{cy5.5}$ (0.84 ns) with increasing concentrations, (Figure 2a,b,c and Table S1, Supporting Information). All the decays were faster than $MN_{cy5.5}$ only, which indicates the presence of dynamic

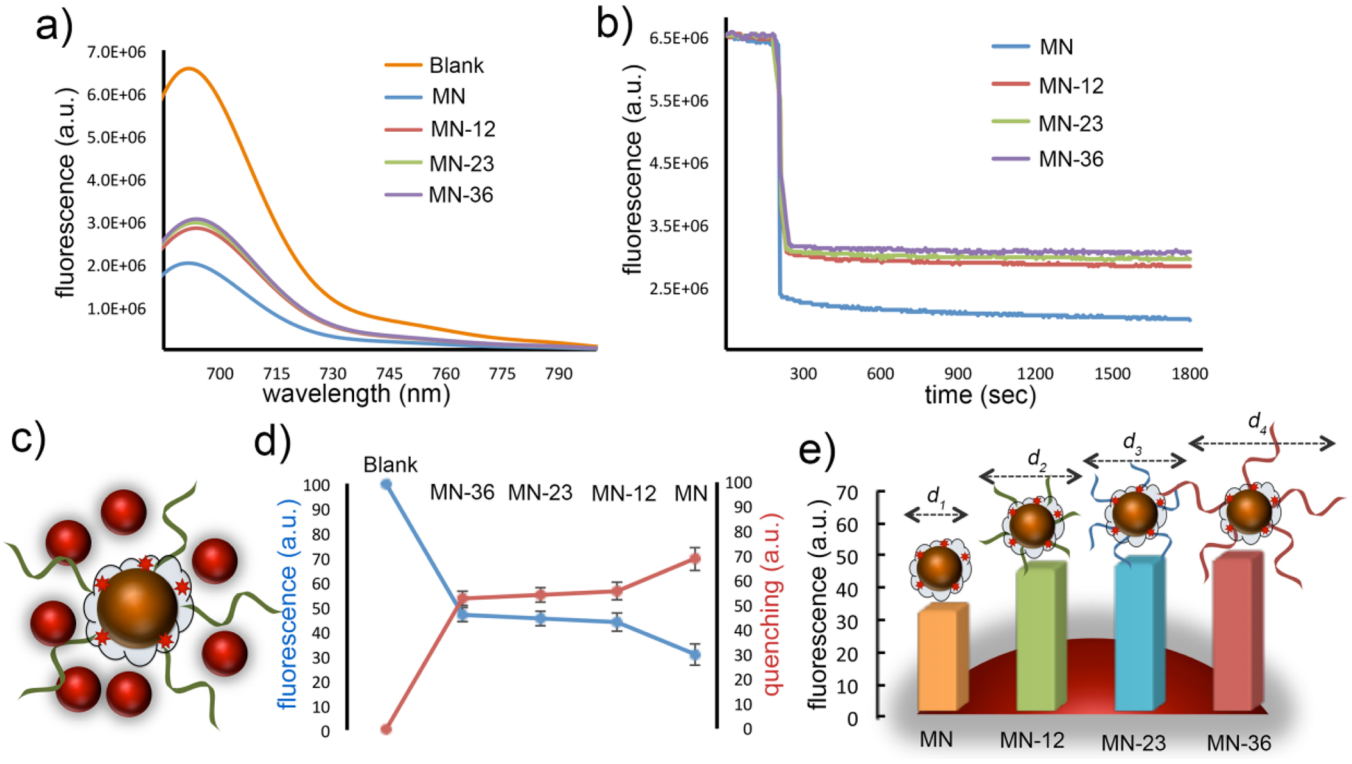

Figure 3. AuNP quenches the fluorescence emission of unmodified or DNA functionalized $MN_{cy5.5}$ compositions (MN, MN-12, MN-23, MN-36). Degree of quenching is determined by change in (a) fluorescence spectra and (b) time-dependent fluorescence measurements at 695 nm. (c) A schematic representation of quenching of $MN_{cy5.5}$-DNA with AuNP. (d, e) The relative fluorescence and quenching (%) intensities with different $MN_{cy5.5}$ compositions and AuNP at minute 30. Note: d1, d2, d3 and d4 represent the hydrodynamic size of the $MN_{cy5.5}$ compositions.

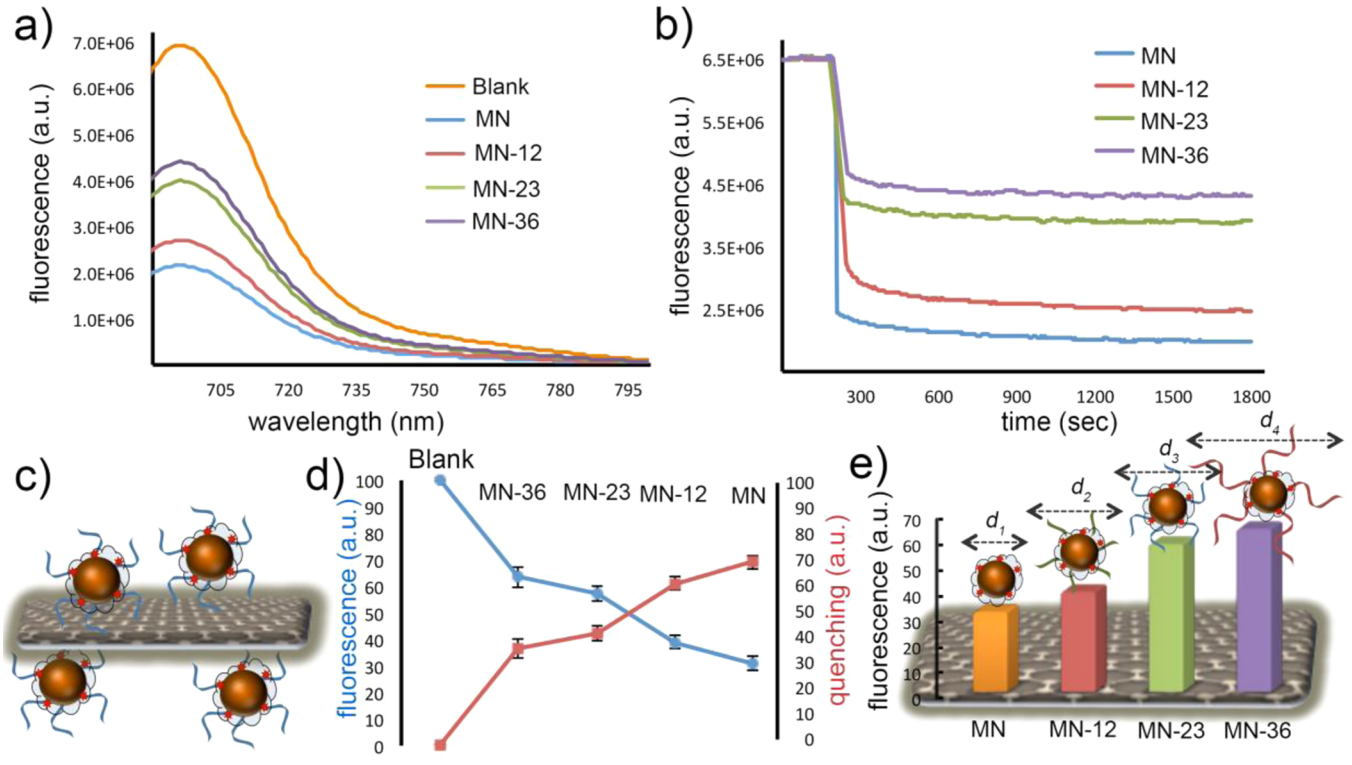

Figure 4. nGO quenches the fluorescence emission of unmodified or DNA functionalized $MN_{cy5.5}$ compositions (MN, MN-12, MN-23, MN-36). Degree of quenching is determined by change in (a) fluorescence spectra and (b) time-dependent fluorescence measurements at 695 nm. (c) A schematic representation of quenching of $MN_{cy5.5}$-DNA with nGO. (d, e) The relative fluorescence and quenching (%) intensities with different $MN_{cy5.5}$ compositions and nGO at minute 30. Note: d1, d2, d3 and d4 represent the hydrodynamic size of the $MN_{cy5.5}$ compositions.

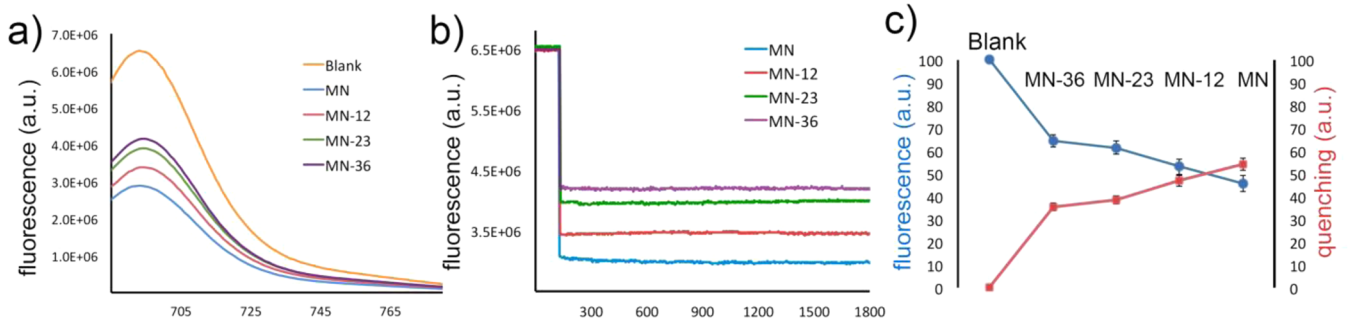

Figure 5. MoS_2 quenches the fluorescence emission of unmodified or DNA functionalized $MN_{cy5.5}$ compositions (MN, MN-12, MN-23, MN-36). Degree of quenching is determined by change in (a) fluorescence spectra and (b) time-dependent fluorescence measurements at 695 nm and (c) the relative fluorescence and quenching (%) intensities with different $MN_{cy5.5}$ compositions and MoS_2 at minute 30.

quenching caused by the nanoquenchers.[23] As discussed above (Figure S1, Supporting Information), after a threshold the change in the fluorescence lifetime lost the linear correlation with increasing concentration, which could be due to the saturation with nanoquenchers, or the presence of different quenching environments possibly due the limited diffusion of spherical or two-dimensional nanoquenchers into the polymer coating of the $MN_{cy5.5}$ with multiple fluorophores (Figures 2d–f).

Afterward, in order to understand the macromolecular spacing effect of immobilized oligonucleotides on the interaction between the nanoquenchers and $MN_{cy5.5}$, we attached three different sizes of single-stranded DNA (ssDNA-12-23-36mer) molecules on the surface of $MN_{cy5.5}$. The dynamic light scattering measurements indicated that the hydrodynamic size of the $MN_{cy5.5}$ increased with the attachment of ssDNA on the surface and a greater increase was observed with longer ssDNA sequences, (Figure S2, Supporting Information). First, we investigated the interaction between the $MN_{cy5.5}$-DNA and unmodified spherical AuNPs, (Figure 3c). The fluorescence emission spectra indicate that AuNPs quench the $MN_{cy5.5}$-DNA dramatically regardless of the size of three different DNA molecules, (Figure 3a). However, a significant difference between the emission spectra of $MN_{cy5.5}$-DNA and bare $MN_{cy5.5}$ was observed. The kinetics studies showed that the quenching of the fluorescence signal is very rapid and stabilizes quickly after titration with AuNP, (Figure 3b). We have also represented our observation by the plotting relative quenching and fluorescence with different $MN_{cy5.5}$ compositions, (Figure 3d,e). The overall observations indicate that there is an efficient and fast quenching of the fluorescence signals in all four cases with a greater quenching efficiency with unmodified $MN_{cy5.5}$. The immobilized oligonucleotides influence the quenching yield of $MN_{cy5.5}$, which, however, was independent of the size of DNAs. We speculate that DNA length-independent quenching of $MN_{cy5.5}$ at these particular DNA sizes could be due to the (1) greater size of $MN_{cy5.5}$ over AuNP and (2) relatively small number of DNAs on the $MN_{cy5.5}$ surface. We postulate that the negatively charged gold nanoparticles can diffuse into the grooves of the positively charged $MN_{cy5.5}$ surface regardless of the size of immobilized DNAs and interfere with the emission of cy5.5 on the surface. Moreover, due to the absorption of ssDNA on AuNP via specific chemical interactions,[15,19] the ssDNA on the $MN_{cy5.5}$-DNA could contribute to the interaction between the nanoparticles.

Later, we investigated the interaction between the $MN_{cy5.5}$-DNA and unmodified planar nGO (Figure 4c). The fluorescence of the different $MN_{cy5.5}$ compositions are significantly affected by extraordinary quenching capability of nGO. We observed that nGO has a higher quenching efficiency on unmodified $MN_{cy5.5}$ compared to the $MN_{cy5.5}$-DNA compositions (Figure 4a). The kinetics studies indicate that the quenching of the fluorescence signal is very fast and stabilizes shortly after the addition of bare nGO (Figure 4b). Unlike gold nanoparticles, the length of the immobilized DNA molecules on $MN_{cy5.5}$-DNA surface played a significant role in altering the magnitude of fluorescence with bare nGO (Figure 4d,e). We postulate that the large two-dimensional planar surface of nGO is unlikely to diffuse into $MN_{cy5.5}$ grooves and interact with the nanoparticle surface. In contrast, the $MN_{cy5.5}$-DNA interacts with the planar surface of the bare nGO, and thus DNA coating creates spacing between surfaces (Figure 4c). Overall, results suggest that the size of the immobilized DNA molecules plays a critical role in separating two nanoparticle surfaces.

Similarly, we studied a graphene-like material, MoS_2, which has common features with GO. MoS_2 is a two-dimensional material that has very recently been investigated due to some exciting physical properties.[47,48] Similar to nGO, MoS_2 is planar and quenches the fluorescence of molecular probes. Here, for the first time, we explored the interaction between MoS_2 and fluorescent nanoparticles, $MN_{cy5.5}$, with a distant-dependent manner using fluorescence spectroscopy. First, we monitored the change in the emission spectra of $MN_{cy5.5}$ and $MN_{cy5.5}$-DNA compositions with MoS_2 titration, (Figure 5a). A DNA-length-dependent difference in fluorescence was observed in all cases. Smaller fluorescence quenching efficiency was observed as the length of DNA molecules was increased. The kinetics studies demonstrated that the quenching occurs very fast and stabilizes rapidly, (Figure 5b). The overall data suggest that (1) the interaction between MoS_2 and $MN_{cy5.5}$ in very similar to the nGO and $MN_{cy5.5}$ interaction, most likely due to the structural similarities and (2) the size of the DNA molecules plays an important role in the quenching efficiency of $MN_{cy5.5}$ fluorescence, (Figure 5c). Furthermore, due to the fast absorption of ssDNA on nGO and MoS_2 surface,[29,48] the ssDNA on $MN_{cy5.5}$-DNA could contribute to the interaction between the interfaces.

Later, we investigated the spacing effect on the relative quenching efficiency when DNA molecules were attached on nanoquenchers, AuNP or nGO, instead of the fluorescent nanoparticle ($MN_{cy5.5}$). First, we studied with DNA function-

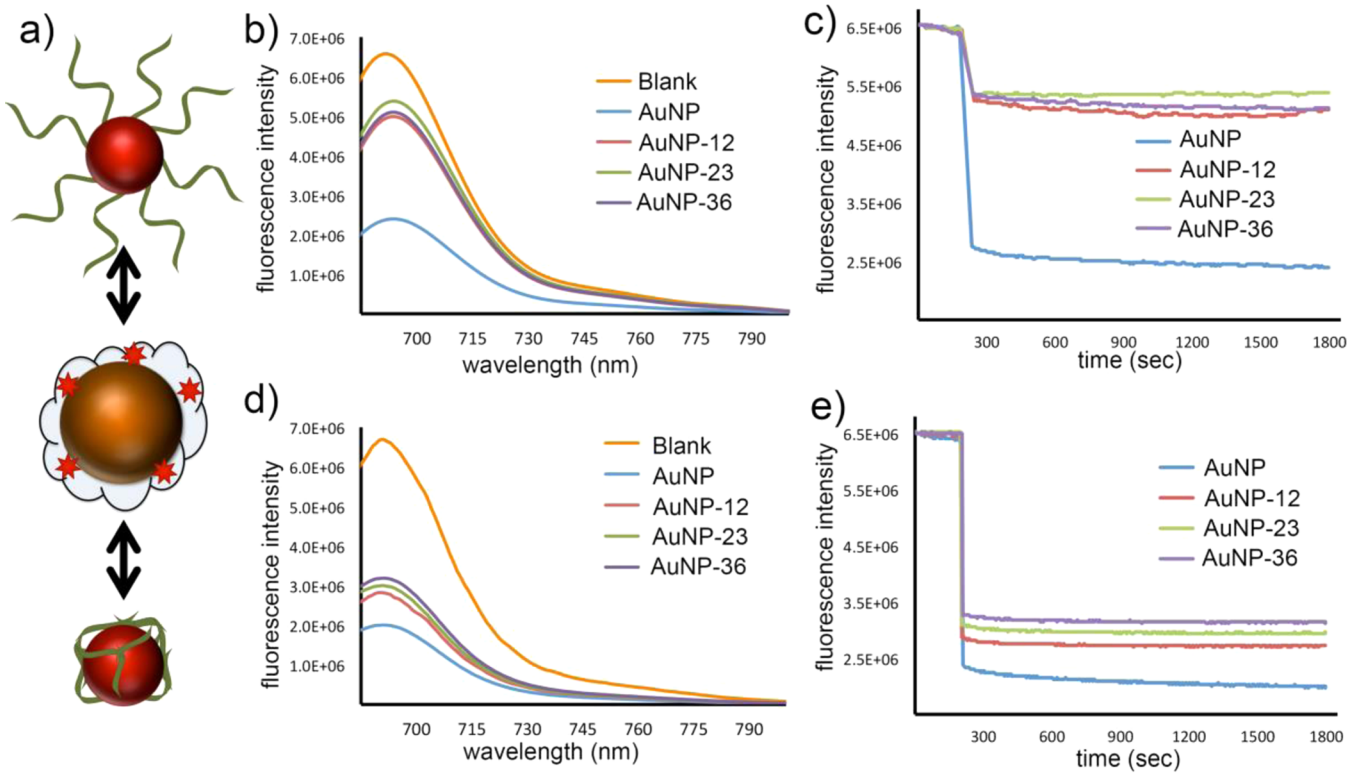

Figure 6. DNA-functionalized AuNP (immobilized or surface adsorbed) quenches the fluorescence emission of unmodified $MN_{cy5.5}$. (a) A schematic representation of quenching of $MN_{cy5.5}$ with AuNP-DNA with two different approaches. Degree of quenching is determined by change in fluorescence spectra of $MN_{cy5.5}$ using (b) immobilization or (d) adsorption approach. Time-dependent fluorescence measurements at 695 nm using (c) immobilization and (e) adsorption approach.

alized gold nanoparticles. Two different attachment approaches were investigated in performing this study, one with anchoring the DNA molecules on the surface via thiol gold chemistry and the second via label-free surface adsorption (Figure 6a). In the first approach, we have observed that unmodified AuNP quenches the fluorescence of $MN_{cy5.5}$ remarkably with a quenching efficiency of 71% ± 1.2. However, the immobilized DNA molecules, independent of the different sizes, dramatically interfere with the quenching of $MN_{cy5.5}$ with an efficiency of 21% ± 3.1 (Figure 6b,c). Although the interference was expected, the similar degree of quenching yield in all DNA sizes was surprising. In the second approach, the DNA molecules were adsorbed onto the AuNP surface using a label-free method, where the adsorbed DNA molecules wrap the gold surface via specific chemical interactions.[15,19] In this approach, we have observed that the surface adsorbed DNA molecules interfere with the interactions between the $MN_{cy5.5}$ and AuNP independent of the size of the DNAs, (Figure 6d,e). However, this effect was significantly lesser than the first approach, (quenching efficiency = 55% ± 3.3) (see Figure S3 in the Supporting Information). We postulate that semistretched DNA molecules on AuNPs in the first approach[20] created a greater shell around spherical gold surface than the DNAs that wrap the AuNPs in the second approach.

Later, we demonstrated a heavy metal ion sensing application using $MN_{cy5.5}$ and AuNPs with/out noncovalently attached oligonucleotides. We monitored the fluorescence intensity of $MN_{cy5.5}$ using mercury aptamer and AuNP with/out of 100 nM mercury ions, (scheme in Figure S4, Supporting Information). In the presence of Hg^{2+}, aptamers bind to Hg^{2+} and do not adsorb on the AuNP surface, whereas in the absence of Hg^{2+}, aptamers wrap the AuNP surface, setting a greater distance between the AuNP and $MN_{cy5.5}$. As a result, in the presence of mercury ions, a greater decrease in fluorescence intensity is observed, (Figure S4, Supporting Information).

Similar to the AuNP study above, we functionalized nGO with two different approaches, covalent immobilization and noncovalent adsorption (Figure 7a). Although the noncovalent attachment was achieved via standard nonspecific adsorption of ssDNA on the surface of nGO, the covalent immobilization was achieved via amide linkages between amine modified DNA molecules and free carboxyl groups of nGO using EDC (*N*-(3-(dimethylamino)propyl)-*N*′-ethylcarbodiimide hydrochloride) chemistry.

To observe the effect of ssDNA between the interactions nGO and $MN_{cy5.5}$, the $MN_{cy5.5}$ was titrated with three different nGO−DNA compositions using both attachment approaches. The change in the fluorescence was monitored overtime and compared to the quenching efficiency of bare nGO. As seen in Figure 7b, regardless of the size of the DNAs, partial quenching in fluorescence intensity was observed upon adding nGO−DNA into $MN_{cy5.5}$ solution, which was significantly lesser when compared to bare nGO and $MN_{cy5.5}$ titration. The similar quenching yield was observed in both attachment approaches (Figure 7b,c). We postulate that DNA molecules cover the surface of nGO due to the $\pi-\pi$ interaction of aromatic groups and serve as a shield between nGO and $MN_{cy5.5}$ surface regardless of their size. The similar observation in the covalent attachment also suggests a related mechanism. However, the rate of the quenching in the covalent immobilization was significantly slower compared to noncovalent attachment, which happened instantaneously (Figure 7d and inset). This

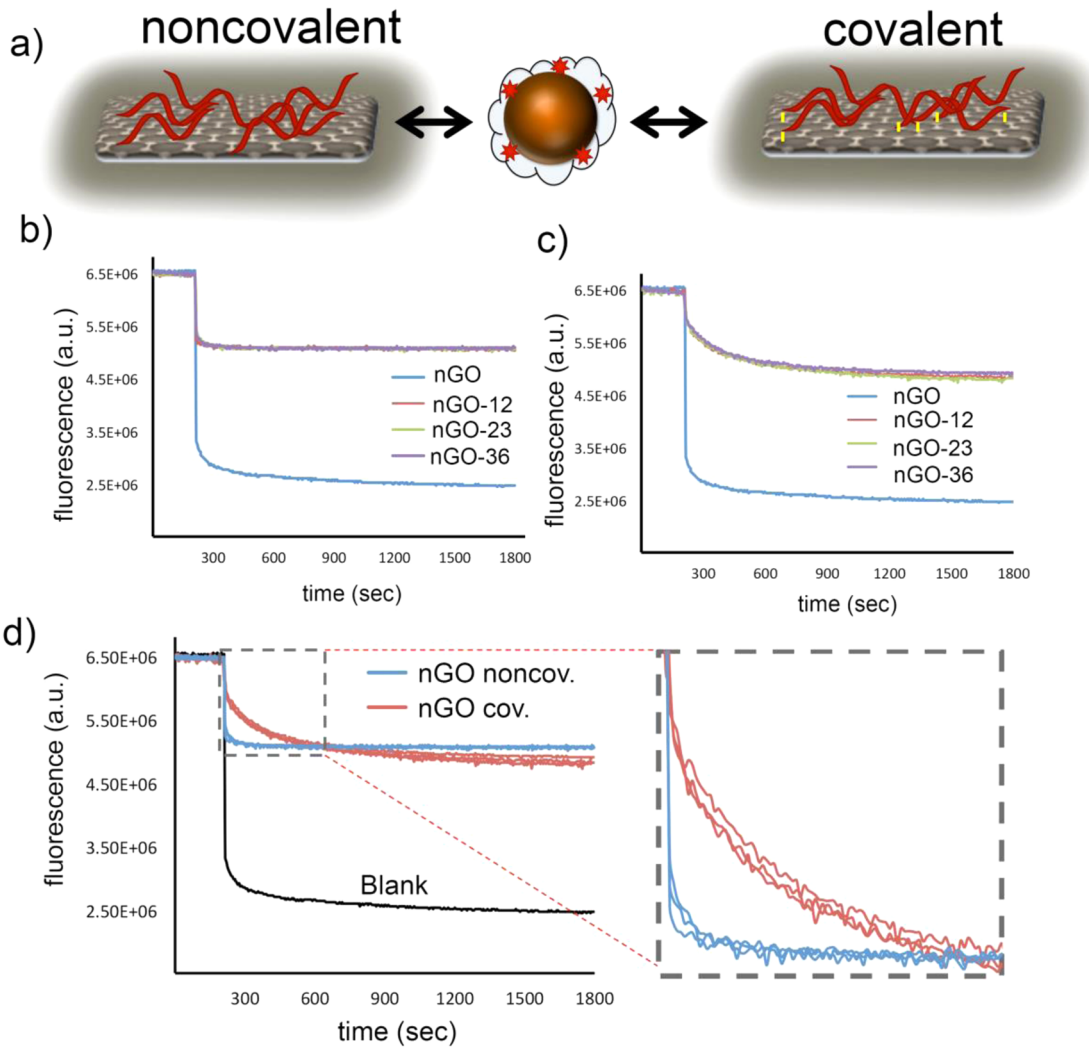

Figure 7. DNA-functionalized nGO (immobilized or surface adsorbed) quenches the fluorescence emission of unmodified $MN_{cy5.5}$. (a) A schematic representation of quenching of $MN_{cy5.5}$ with nGO−DNA with two different approaches. Degree of quenching is determined by change in time-dependent fluorescence measurements at 695 using (b) adsorption or (c) immobilization approach. (d) The rate of the quenching in immobilization approach is slower than the adsorption approach.

might be due to the immobile rigid end of the DNA on nGO surface hindering fast adsorption of $MN_{cy5.5}$, whereas in noncovalent adsorption, the DNA molecules have more freedom of motion. Overall, the final quenching efficiency with all three sizes of DNA and attachment approaches was determined to be approximately 20% and was much smaller than the unmodified nGO-induced quenching. The covalently or noncovalently attached ssDNA molecules on nGO and AuNP have a high binding affinity to both surfaces,[4] therefore we did not observe any displacement of ssDNA by $MN_{cy5.5}$ over time as suggested by the stabilized fluorescence intensities in Figures 4b,c, 6b and 7b,c. The quenching efficiency of each nanoquencher composition on the fluorescence of $MN_{cy5.5}$ is compared in Figures S5 and S6 (Supporting Information). Finally, in order demonstrate the nanoquenchers' capability in quenching the fluorescence of the free fluorophore, we incubated cy5.5 with AuNP, nGO or MoS_2. Fluorescence quenching of free cy5.5 with nanoquenchers is presented in Figure S7 (Supporting Information).

4. CONCLUSION

In summary, we investigated the interaction between fluorescently labeled iron oxide nanoparticles ($MN_{cy5.5}$) and AuNP, nGO or MoS_2 by monitoring the degree of fluorescence quenching with a distance-dependent manner. The spacing between nanoparticle interfaces and the efficiency of fluorescence quenching were controlled by surface functionalized ssDNA molecules. Attachment of DNAs on nanoparticle surfaces was achieved with two different methods: immobilization or adsorption. We have observed that even though the presence of DNA affected the efficiency of quenching in all combinations, regardless of the attachment procedure, the length of DNAs did not always matter. We have demonstrated that nGO and MoS_2, both having similarities in their two-dimensional planar structures, display relatively efficient quenching dependent on the size of DNA molecules immobilized on the $MN_{cy5.5}$ surface. On the other hand, when DNA molecules were attached on the nGO surface instead of $MN_{cy5.5}$, the presence of the DNAs between 12 and 36 nucleobases long, but not the size, affected the fluorescence quenching efficiency. We have also observed that the spherical

AuNP quenches the fluorescence of $MN_{cy5.5}$ regardless of the size of the DNA molecules on either surface. Whereas the immobilized DNA molecules on AuNP affects the quenching efficiency the utmost.

Overall, the presence of DNA molecules influences the fluorescence emission of fluorescently labeled magnetic nanoparticles dramatically with three different nanoquenchers. The three-dimensional structure of interacting nanoparticles and the attachment procedure of DNAs onto nanoparticle surface play important role in the quenching efficiency. We believe this study could provide important information about engineering hybrid bionanomaterials with tunable optical properties.

■ ASSOCIATED CONTENT

Ⓢ Supporting Information

Additional experimental results and nanoparticle characterizations including titration of $MN_{cy5.5}$ with different concentrations of AuNP, nGO and MoS_2; results of fluorescence lifetime decay fitting into a double exponential model; change in the hydrodynamic size of the $MN_{cy5.5}$ compositions with different lengths of ssDNA measured by dynamic light scattering (DLS) measurements; DNA-functionalized AuNP (immobilized or surface adsorbed) quenching the fluorescence emission of unmodified $MN_{cy5.5}$; quenching of the fluorescence of $MN_{cy5.5}$ with AuNPs in the presence of single stranded mercury aptamer with or without Hg^{2+}; quenching of $MN_{cy5.5}$ with AuNP, nGO or MoS_2 in the presence and absence of oligonucleotide attachments; quenching efficiency of different nanoquencher compositions against fluorescence emission of $MN_{cy5.5}$ and its DNA conjugates with different attachment approaches; quenching of free cy5.5 dye with 4 nM AuNP, 1.8 μg/mL of nGO or 20 μg/mL of MoS_2; absorbance spectrum of 76 nM $MN_{cy5.5}$, 4nM AuNP, 16 μg/mL of nGO and 4.5 μg/mL of MoS_2. This material is available free of charge via the Internet at http://pubs.acs.org.

■ AUTHOR INFORMATION

Corresponding Author

*M. V. Yigit. Tel: (1) 518-442-3002. E-mail: myigit@albany.edu.

Notes

The authors declare no competing financial interest.

■ ACKNOWLEDGMENTS

We thank Kevin Musick and Dr. Kathleen Dunn for the TEM micrographs. We acknowledge the Ministry of National Education, Republic of Turkey, for financial support to Mustafa Balcioglu with full fellowship during his doctoral studies. This work was supported by the SUNY Albany Start-Up Funds.

■ REFERENCES

(1) Wei, Q.; Nagi, R.; Sadeghi, K.; Feng, S.; Yan, E.; Ki, S. J.; Caire, R.; Tseng, D.; Ozcan, A. Detection and Spatial Mapping of Mercury Contamination in Water Samples Using a Smart-Phone. *ACS Nano* **2014**, *8*, 1121−1129.

(2) Hamner, K. L.; Maye, M. M. Thermal Aggregation Properties of Nanoparticles Modified with Temperature Sensitive Copolymers. *Langmuir* **2013**, *29*, 15217−15223.

(3) Huang, H.; Song, W.; Chen, G.; Reynard, J. M.; Ohulchanskyy, T. Y.; Prasad, P. N.; Bright, F. V.; Lovell, J. F. Pd-Porphyrin-Cross-Linked Implantable Hydrogels with Oxygen-Responsive Phosphorescence. *Adv. Healthcare Mater.* **2014**, *3*, 891−896.

(4) Liu, J. Adsorption of DNA onto Gold Nanoparticles and Graphene Oxide: Surface Science and Applications. *Phys. Chem. Chem. Phys.* **2012**, *14*, 10485−10496.

(5) Piao, Y.; Liu, F.; Seo, T. S. A Novel Molecular Beacon Bearing a Graphite Nanoparticle as a Nanoquencher for in Situ mRNA Detection in Cancer Cells. *ACS Appl. Mater. Interfaces* **2012**, *4*, 6785−6789.

(6) Li, J.-L.; Tang, B.; Yuan, B.; Sun, L.; Wang, X.-G. A Review of Optical Imaging and Therapy Using Nanosized Graphene and Graphene Oxide. *Biomaterials* **2013**, *34*, 9519−9534.

(7) Morales-Narvaez, E.; Merkoci, A. Graphene Oxide as an Optical Biosensing Platform. *Adv. Mater.* **2012**, *24*, 3298−3308.

(8) Yigit, M. V.; Zhu, L.; Ifediba, M. A.; Zhang, Y.; Carr, K.; Moore, A.; Medarova, Z. Noninvasive MRI-SERS Imaging in Living Mice Using an Innately Bimodal Nanomaterial. *ACS Nano* **2010**, *5*, 1056−1066.

(9) Wang, P.; Yigit, M. V.; Medarova, Z.; Wei, L.; Dai, G.; Schuetz, C.; Moore, A. Combined Small Interfering RNA Therapy and in Vivo Magnetic Resonance Imaging in Islet Transplantation. *Diabetes* **2011**, *60*, 565−571.

(10) Alexander, C. M.; Maye, M. M.; Dabrowiak, J. C. DNA-Capped Nanoparticles Designed for Doxorubicin Drug Delivery. *Chem. Commun. (Cambridge, U. K.)* **2011**, *47*, 3418−3420.

(11) Alexander, C. M.; Dabrowiak, J. C.; Maye, M. M. Investigation of the Drug Binding Properties and Cytotoxicity of DNA-Capped Nanoparticles Designed as Delivery Vehicles for the Anticancer Agents Doxorubicin and Actinomycin D. *Bioconjugate Chem.* **2012**, *23*, 2061−2070.

(12) Hamner, K. L.; Alexander, C. M.; Coopersmith, K.; Reishofer, D.; Provenza, C.; Maye, M. M. Using Temperature-Sensitive Smart Polymers to Regulate DNA-Mediated Nanoassembly and Encoded Nanocarrier Drug Release. *ACS Nano* **2013**, *7*, 7011−7020.

(13) Kundu, A.; Layek, R. K.; Kuila, A.; Nandi, A. K. Highly Fluorescent Graphene Oxide-Poly(vinyl alcohol) Hybrid: An Effective Material for Specific Au^{3+} Ion Sensors. *ACS Appl. Mater. Interfaces* **2012**, *4*, 5576−5582.

(14) Bunz, U. H.; Rotello, V. M. Gold Nanoparticle-Fluorophore Complexes: Sensitive and Discerning "Noses" for Biosystems Sensing. *Angew. Chem., Int. Ed.* **2010**, *49*, 3268−3279.

(15) Xia, F.; Zuo, X.; Yang, R.; Xiao, Y.; Kang, D.; Vallee-Belisle, A.; Gong, X.; Yuen, J. D.; Hsu, B. B.; Heeger, A. J.; Plaxco, K. W. Colorimetric Detection of DNA, Small Molecules, Proteins, and Ions Using Unmodified Gold Nanoparticles and Conjugated Polyelectrolytes. *Proc. Natl. Acad. Sci. U. S. A.* **2010**, *107*, 10837−10841.

(16) Yang, L.; Liu, C.; Ren, W.; Li, Z. Graphene Surface-Anchored Fluorescence Sensor for Sensitive Detection of Microrna Coupled with Enzyme-Free Signal Amplification of Hybridization Chain Reaction. *ACS Appl. Mater. Interfaces* **2012**, *4*, 6450−6453.

(17) Chou, S. S.; De, M.; Luo, J.; Rotello, V. M.; Huang, J.; Dravid, V. P. Nanoscale Graphene Oxide (nGO) as Artificial Receptors: Implications for Biomolecular Interactions and Sensing. *J. Am. Chem. Soc.* **2012**, *134*, 16725−16733.

(18) Stobiecka, M.; Hepel, M. Multimodal Coupling of Optical Transitions and Plasmonic Oscillations in Rhodamine B Modified Gold Nanoparticles. *Phys. Chem. Chem. Phys.* **2011**, *13*, 1131−1139.

(19) Li, H.; Rothberg, L. Colorimetric Detection of DNA Sequences Based on Electrostatic Interactions with Unmodified Gold Nanoparticles. *Proc. Natl. Acad. Sci. U. S. A.* **2004**, *101*, 14036−14039.

(20) Parak, W. J.; Pellegrino, T.; Micheel, C. M.; Gerion, D.; Williams, S. C.; Alivisatos, A. P. Conformation of Oligonucleotides Attached to Gold Nanocrystals Probed by Gel Electrophoresis. *Nano Lett.* **2002**, *3*, 33−36.

(21) Dulkeith, E.; Ringler, M.; Klar, T. A.; Feldmann, J.; Munoz Javier, A.; Parak, W. J. Gold Nanoparticles Quench Fluorescence by Phase Induced Radiative Rate Suppression. *Nano Lett.* **2005**, *5*, 585−589.

(22) Chhabra, R.; Sharma, J.; Wang, H.; Zou, S.; Lin, S.; Yan, H.; Lindsay, S.; Liu, Y. Distance-Dependent Interactions between Gold

Nanoparticles and Fluorescent Molecules with DNA as Tunable Spacers. *Nanotechnology* **2009**, *20*, 485201.
(23) Huang, P.-J. J.; Liu, J. DNA-Length-Dependent Fluorescence Signaling on Graphene Oxide Surface. *Small* **2012**, *8*, 977−983.
(24) Mao, H. Y.; Laurent, S.; Chen, W.; Akhavan, O.; Imani, M.; Ashkarran, A. A.; Mahmoudi, M. Graphene: Promises, Facts, Opportunities, and Challenges in Nanomedicine. *Chem. Rev.* **2013**, *113*, 3407−3424.
(25) Geim, A. K. Graphene: Status and Prospects. *Science* **2009**, *324*, 1530−1534.
(26) Novoselov, K. S.; Geim, A. K.; Morozov, S. V.; Jiang, D.; Zhang, Y.; Dubonos, S. V.; Grigorieva, I. V.; Firsov, A. A. Electric Field Effect in Atomically Thin Carbon Films. *Science* **2004**, *306*, 666−669.
(27) Geim, A. K.; Novoselov, K. S. The Rise of Graphene. *Nat. Mater.* **2007**, *6*, 183−191.
(28) Chung, C.; Kim, Y. K.; Shin, D.; Ryoo, S. R.; Hong, B. H.; Min, D. H. Biomedical Applications of Graphene and Graphene Oxide. *Acc. Chem. Res.* **2013**, *46*, 2211−2224.
(29) Rana, M.; Balcioglu, M.; Robertson, N.; Yigit, M. V. Nano-Graphene Oxide as a Novel Platform for Monitoring the Effect of LNA Modification on Nucleic Acid Interactions. *Analyst* **2014**, *139*, 714−720.
(30) Li, S.; Aphale, A. N.; Macwan, I. G.; Patra, P. K.; Gonzalez, W. G.; Miksovska, J.; Leblanc, R. M. Graphene Oxide as a Quencher for Fluorescent Assay of Amino Acids, Peptides, and Proteins. *ACS Appl. Mater. Interfaces* **2012**, *4*, 7069−7075.
(31) Balcioglu, M.; Rana, M.; Yigit, M. V. Doxorubicin Loading on Graphene Oxide, Iron Oxide and Gold Nanoparticle Hybrid. *J. Mater. Chem. B* **2013**, *1*, 6187−6193.
(32) Li, F.; Pei, H.; Wang, L. H.; Lu, J. X.; Gao, J. M.; Jiang, B. W.; Zhao, X. C.; Fan, C. H. Nanomaterial-Based Fluorescent DNA Analysis: A Comparative Study of the Quenching Effects of Graphene Oxide, Carbon Nanotubes, and Gold Nanoparticles. *Adv. Funct. Mater.* **2013**, *23*, 4140−4148.
(33) Wang, Y.; Li, Z.; Wang, J.; Li, J.; Lin, Y. Graphene and Graphene Oxide: Biofunctionalization and Applications in Biotechnology. *Trends Biotechnol.* **2011**, *29*, 205−212.
(34) Fu, X.; Lou, T.; Chen, Z.; Lin, M.; Feng, W.; Chen, L. "Turn-on" Fluorescence Detection of Lead Ions Based on Accelerated Leaching of Gold Nanoparticles on the Surface of Graphene. *ACS Appl. Mater. Interfaces* **2012**, *4*, 1080−1086.
(35) Liu, Y. M.; Punckt, C.; Pope, M. A.; Gelperin, A.; Aksay, I. A. Electrochemical Sensing of Nitric Oxide with Functionalized Graphene Electrodes. *ACS Appl. Mater. Interfaces* **2013**, *5*, 12624−12630.
(36) He, Y.; Huang, G.; Cui, H. Quenching the Chemiluminescence of Acridinium Ester by Graphene Oxide for Label-Free and Homogeneous DNA Detection. *ACS Appl. Mater. Interfaces* **2013**, *5*, 11336−11340.
(37) Shi, Y.; Yi, C.; Zhang, Z.; Zhang, H.; Li, M.; Yang, M.; Jiang, Q. Peptide-Bridged Assembly of Hybrid Nanomaterial and Its Application for Caspase-3 Detection. *ACS Appl. Mater. Interfaces* **2013**, *5*, 6494−6501.
(38) Dey, R. S.; Raj, C. R. Redox-Functionalized Graphene Oxide Architecture for the Development of Amperometric Biosensing Platform. *ACS Appl. Mater. Interfaces* **2013**, *5*, 4791−4798.
(39) Ryoo, S.-R.; Lee, J.; Yeo, J.; Na, H.-K.; Kim, Y.-K.; Jang, H.; Lee, J. H.; Han, S. W.; Lee, Y.; Kim, V. N.; Min, D.-H. Quantitative and Multiplexed Microrna Sensing in Living Cells Based on Peptide Nucleic Acid and Nano Graphene Oxide (Pango). *ACS Nano* **2013**, *7*, 5882−5891.
(40) Dong, H.; Ding, L.; Yan, F.; Ji, H.; Ju, H. The Use of Polyethylenimine-Grafted Graphene Nanoribbon for Cellular Delivery of Locked Nucleic Acid Modified Molecular Beacon for Recognition of Microrna. *Biomaterials* **2011**, *32*, 3875−3882.
(41) Reed, J. C.; Zhu, H.; Zhu, A. Y.; Li, C.; Cubukcu, E. Graphene-Enabled Silver Nanoantenna Sensors. *Nano Lett.* **2012**, *12*, 4090−4094.
(42) Tang, L.; Wang, Y.; Liu, Y.; Li, J. DNA-Directed Self-Assembly of Graphene Oxide with Applications to Ultrasensitive Oligonucleotide Assay. *ACS Nano* **2011**, *5*, 3817−3822.
(43) Ryoo, S. R.; Lee, J.; Yeo, J.; Na, H. K.; Kim, Y. K.; Jang, H.; Lee, J. H.; Han, S. W.; Lee, Y.; Kim, V. N.; Min, D. H. Quantitative and Multiplexed Microrna Sensing in Living Cells Based on Peptide Nucleic Acid and Nano Graphene Oxide (Pango). *ACS Nano* **2013**, *7*, 5882−5891.
(44) Kim, H.; Namgung, R.; Singha, K.; Oh, I. K.; Kim, W. J. Graphene Oxide-Polyethylenimine Nanoconstruct as a Gene Delivery Vector and Bioimaging Tool. *Bioconjugate Chem.* **2011**, *22*, 2558−2567.
(45) Xu, C.; Yang, D.; Mei, L.; Lu, B.; Chen, L.; Li, Q.; Zhu, H.; Wang, T. Encapsulating Gold Nanoparticles or Nanorods in Graphene Oxide Shells as a Novel Gene Vector. *ACS Appl. Mater. Interfaces* **2013**, *5*, 2715−2724.
(46) Shen, H.; Liu, M.; He, H.; Zhang, L.; Huang, J.; Chong, Y.; Dai, J.; Zhang, Z. PEGylated Graphene Oxide-Mediated Protein Delivery for Cell Function Regulation. *ACS Appl. Mater. Interfaces* **2012**, *4*, 6317−6323.
(47) Liu, H.; Si, M.; Deng, Y.; Neal, A. T.; Du, Y.; Najmaei, S.; Ajayan, P. M.; Lou, J.; Ye, P. D. Switching Mechanism in Single-Layer Molybdenum Disulfide Transistors: An Insight into Current Flow across Schottky Barriers. *ACS Nano* **2014**, *8*, 1031−1038.
(48) Zhu, C.; Zeng, Z.; Li, H.; Li, F.; Fan, C.; Zhang, H. Single-Layer MoS_2-Based Nanoprobes for Homogeneous Detection of Biomolecules. *J. Am. Chem. Soc.* **2013**, *135*, 5998−6001.
(49) Liu, T.; Wang, C.; Gu, X.; Gong, H.; Cheng, L.; Shi, X.; Feng, L.; Sun, B.; Liu, Z. Drug Delivery with PEGylated MoS Nano-Sheets for Combined Photothermal and Chemotherapy of Cancer. *Adv. Mater.* **2014**, *26*, 3433−3440.
(50) Wei, Q.; Qi, H.; Luo, W.; Tseng, D.; Ki, S. J.; Wan, Z.; Gorocs, Z.; Bentolila, L. A.; Wu, T. T.; Ozcan, A. Fluorescent Imaging of Single Nanoparticles and Viruses on a Smart Phone. *ACS Nano* **2013**, *7*, 9147−9155.
(51) Hennequin, Y.; Allier, C. P.; McLeod, E.; Mudanyali, O.; Migliozzi, D.; Ozcan, A.; Dinten, J. M. Optical Detection and Sizing of Single Nanoparticles Using Continuous Wetting Films. *ACS Nano* **2013**, *7*, 7601−7609.
(52) Rana, M.; Balcioglu, M.; Yigit, M. V. Locked Nucleic Acid-Modified Antisense Mir-10b Oligonucleotides Form Stable Duplexes on Gold Nanoparticles. *Bionanoscience* **2014**, *4*, 195−200.
(53) Swierczewska, M.; Lee, S.; Chen, X. The Design and Application of Fluorophore-Gold Nanoparticle Activatable Probes. *Phys. Chem. Chem. Phys.* **2011**, *13*, 9929−9941.
(54) Ling, J.; Huang, C. Z. Energy Transfer with Gold Nanoparticles for Analytical Applications in the Fields of Biochemical and Pharmaceutical Sciences. *Anal. Methods* **2010**, *2*, 1439−1447.
(55) Fan, C.; Wang, S.; Hong, J. W.; Bazan, G. C.; Plaxco, K. W.; Heeger, A. J. Beyond Superquenching: Hyper-Efficient Energy Transfer from Conjugated Polymers to Gold Nanoparticles. *Proc. Natl. Acad. Sci. U. S. A.* **2003**, *100*, 6297−6301.
(56) Tu, Y.; Wu, P.; Zhang, H.; Cai, C. Fluorescence Quenching of Gold Nanoparticles Integrating with a Conformation-Switched Hairpin Oligonucleotide Probe for Microrna Detection. *Chem. Commun. (Cambridge, U. K.)* **2012**, *48*, 10718−10720.
(57) Acar, H.; Genc, R.; Urel, M.; Erkal, T. S.; Dana, A.; Guler, M. O. Self-Assembled Peptide Nanofiber Templated One-Dimensional Gold Nanostructures Exhibiting Resistive Switching. *Langmuir* **2012**, *28*, 16347−16354.
(58) Han, H.; Valle, V.; Maye, M. M. Probing Resonance Energy Transfer and Inner Filter Effects in Quantum Dot−Large Metal Nanoparticle Clusters Using a DNA-Mediated Quench and Release Mechanism. *J. Phys. Chem. C* **2012**, *116*, 22996−23003.
(59) Han, H.; Valle, V.; Maye, M. M. Probing the Quenching of CdSe/ZnS Qdots by Au, Au/Ag, and Au/Pd Nanoparticles. *Nanotechnology* **2012**, *23*, 435401.

(60) Herne, T. M.; Tarlov, M. J. Characterization of DNA Probes Immobilized on Gold Surfaces. *J. Am. Chem. Soc.* **1997**, *119*, 8916−8920.
(61) Tassa, C.; Shaw, S. Y.; Weissleder, R. Dextran-Coated Iron Oxide Nanoparticles: A Versatile Platform for Targeted Molecular Imaging, Molecular Diagnostics, and Therapy. *Acc. Chem. Res.* **2011**, *44*, 842−852.
(62) Yigit, M. V.; Mazumdar, D.; Lu, Y. MRI Detection of Thrombin with Aptamer Functionalized Superparamagnetic Iron Oxide Nanoparticles. *Bioconjugate Chem.* **2008**, *19*, 412−417.
(63) Yigit, M. V.; Mazumdar, D.; Kim, H. K.; Lee, J. H.; Odintsov, B.; Lu, Y. Smart "Turn-on" Magnetic Resonance Contrast Agents Based on Aptamer-Functionalized Superparamagnetic Iron Oxide Nanoparticles. *ChemBioChem* **2007**, *8*, 1675−1678.
(64) Sulek, S.; Mammadov, B.; Mahcicek, D. I.; Sozeri, H.; Atalar, E.; Tekinay, A. B.; Guler, M. O. Peptide Functionalized Superparamagnetic Iron Oxide Nanoparticles as MRI Contrast Agents. *J. Mater. Chem.* **2011**, *21*, 15157−15162.
(65) Yigit, M. V.; Moore, A.; Medarova, Z. Magnetic Nanoparticles for Cancer Diagnosis and Therapy. *Pharm. Res.* **2012**, *29*, 1180−1188.
(66) Medarova, Z.; Pham, W.; Farrar, C.; Petkova, V.; Moore, A. In Vivo Imaging of siRNA Delivery and Silencing in Tumors. *Nat. Med.* **2007**, *13*, 372−377.
(67) Pittet, M. J.; Swirski, F. K.; Reynolds, F.; Josephson, L.; Weissleder, R. Labeling of Immune Cells for in Vivo Imaging Using Magnetofluorescent Nanoparticles. *Nat. Protoc.* **2006**, *1*, 73−79.
(68) Yigit, M. V.; Ghosh, S. K.; Kumar, M.; Petkova, V.; Kavishwar, A.; Moore, A.; Medarova, Z. Context-Dependent Differences in miR-10b Breast Oncogenesis Can Be Targeted for the Prevention and Arrest of Lymph Node Metastasis. *Oncogene* **2013**, *32*, 1530−1538.
(69) Kumar, M.; Yigit, M.; Dai, G.; Moore, A.; Medarova, Z. Image-Guided Breast Tumor Therapy Using a Small Interfering RNA Nanodrug. *Cancer Res.* **2010**, *70*, 7553−7561.
(70) Liu, J.; Lu, Y. Preparation of Aptamer-Linked Gold Nanoparticle Purple Aggregates for Colorimetric Sensing of Analytes. *Nat. Protoc.* **2006**, *1*, 246−252.